Regular Article

PHYSICAL CHEMISTRY RESEARCH
Published by the
Iranian Chemical Society
www.physchemres.org
info@physchemres.org

*Phys. Chem. Res., Vol. 12, No. 4, 1019-1035, December 2024*
**DOI: 10.22036/pcr.2024.446502.2487**

# Computational Investigation of the Stability and Efficiency of Indenoindene-based A-π-D-π-A Type Compounds in Organic Photovoltaics Cells

H. Etabti[a,*], U. Ali[b], A. Fitri[a], A. Touimi Benjelloun[a], R. Kacimi[c], M. Benzakour[a] and M. Mcharfi[a]

[a]*LIMAS, Faculty of Sciences Dhar El Mahraz, Sidi Mohamed Ben Abdellah University, Fez, Morocco*

[b]*Laser Center, Institute of Physical Chemistry of Polish Academy of Sciences (IChF PAN) 44/52, Marcina Kasparzka 01-224, Warsaw, R. Poland*

[c]*CMC-Molecular Chemistry and Natural Substances Laboratory, Faculty of Sciences, University Moulay Ismail, Meknes, Morocco*

*(Received 2 March 2024, Accepted 31 July 2024)*

This paper analyzes the computational aspects of a planar non-fullerene acceptor, specifically indenoindene (IDTIC-4F), in the context of organic solar cell production. The B3LYP/6-31G(d,p) and TD-B3LYP/6-31G(d,p) methods are identified for predicting optoelectronic properties, with calculations comparing HOMO and LUMO energies, $E_{gap}$, $\lambda_{max}$ to experimental results. Illustrative techniques, including TDM, RDG, ELF analysis, and hole-electron isosurface, depict electronic excitation processes and electron-hole positioning. The study evaluates IDTIC-4F as an electron donor alongside fullerenes and their derivatives, revealing varied $V_{oc}$ values (0.754 to 1.254 V). Emphasizing IDTIC-4F's substantial potential, the research suggests its promising viability as an electron donor for solar cell integration.

**Keywords:** Indenoindene, A-D-π-D-A, DFT and TD-DFT analysis, Open-circuit voltage, Organic solar cells

## INTRODUCTION

The energy problem is today's most pressing and intriguing topic [1]. Over the last few decades, urbanization [2], industrialization [3], and population growth [4] have greatly increased energy consumption. Fossil fuels such as oil, gas, and coal now dominate worldwide energy acquisition, while renewable resources such as hydropower, wind, solar, biofuels, and others lag behind [5].

Renewable energy appears as a noteworthy solution to a variety of energy-related issues [6]. Solar energy stands out as the most promising renewable source due to its tremendous energy potential and minimal carbon footprint, accounting for only 1.1% of total emissions. Photovoltaics, when triggered by sunlight, create electrical energy, making solar energy a sustainable, environmentally benign, easily deployable, plentiful, and cost-effective renewable energy source [7-10]. For many decades, inorganic and silicon-based solar cells dominated the photovoltaic industry due to their high power conversion efficiencies (PCE) of 15% to 20% [11]. Despite their excellent efficiency, the high production costs, difficult manufacturing methods, and inability to manage energy levels led the way for the development of organic solar cells [12].

Organic solar cells may be easily manufactured using simple and inexpensive technologies such as sputter deposition, spin coating, printing, and different roll-to-roll production techniques [13]. These organic devices outperform their inorganic counterparts because of their high optical absorption coefficient, unique structure, ease of integration, and changing energy levels [14,15].

In bulk heterojunction organic solar cells (BHJ), a blended zone comprising donor and acceptor materials sits between two layers of electrodes. Following radiation absorption, this mechanism produces an electron-hole pair known as an exciton [16]. The degree of exciton dissociation and the efficient transfer of dissociated charges to their respective electrodes both have a major impact on solar cell efficiency [17]. Furthermore, the fill factor (FF), open-circuit voltage ($V_{oc}$), and short-circuit current density ($J_{sc}$) are critical in

*Corresponding author. E-mail: hanane.etabti@usmba.ac.ma

determining the efficiency of organic solar cells (OSCs) [18]. While fullerene materials and their derivatives, particularly [6,6]-phenyl butyric acid methyl ester ($PC_{61}BM$ and $PC_{71}BM$), are often used as acceptors in organic solar cells (OSCs), their application in the photovoltaic industry is limited due to factors such as their compact structure, non-tunable energy levels, limited absorption range, low open-circuit voltage ($V_{oc}$), and high production costs [19].

Donor-acceptor semiconductors can be built in a variety of topologies to maximize their electrical characteristics. Linear D-A-D designs have donor units flanking a central acceptor, which promotes efficient charge transfer. Star-shaped structures combine a central acceptor with many donor arms to improve charge separation and transport. Coplanar topologies organize donor and acceptor units in a planar form, allowing for π-π stacking and improved charge mobility. Additionally, D-A block copolymers integrate donor and acceptor blocks in a single polymer chain, resulting in balanced charge transfer. Finally, dendritic architectures have a central core with branching donor-acceptor units, resulting in a larger surface area and better NLO characteristics [20-22].

The acceptor-donor-acceptor (A-D-A) framework is a well-established technique in the field of non-fullerene acceptors (NFAs). This is due to its adjustable optical bandgap, changeable LUMO and HOMO energy levels, high thermal stability, and significant absorption capabilities in both the visible and near-infrared regions [23-26]. Power conversion efficiencies (PCEs) of organic solar cells (OSCs) utilizing acceptors of the acceptor-donor-acceptor (A-D-A) type have increased rapidly in recent years, topping 14%, thanks to material transformation and device optimization. Furthermore, advancements in molecular drift and absorption have led to the development of A-π-D-π-A-type acceptors with varied donor-acceptor connections [27,28]. As a result, tandem devices using these architectures have attained power conversion efficiencies (PCEs) greater than 18% [16-19].

In our current investigation, the polymer indenoindene was chosen as a typical electron-donating substance. This decision was made due to its good solubility in nonaromatic solvents, simple planar structure, strong UV-visible absorptions, and close proximity to end-capping groups, which act as electron acceptors in the creation of organic photovoltaic (OPV) cells. Inspired by recent studies on indandione and benzodithiophene, we focused on studying the structural, optical, and electrical properties of a molecule developed and synthesized by Zulfiqar *et al.* [29].

Throughout the manuscript, we will refer to this compound as IDTIC-4F for simplicity. Its selection is grounded in its straightforward synthesis and the capacity for chemical modification of the ring acceptor moieties. This modification has the potential to influence various material properties, including HOMO, $E_{gap}$, photoluminescence spectra, and more. The recently developed high-efficiency compound, IDTIC-4F, characterized by a central fused ring (indenoindene core), underwent modifications to its alkyl side chains. Additionally, an acceptor group was introduced at the exterior to augment its electron-withdrawing capability (refer to Fig. 1).

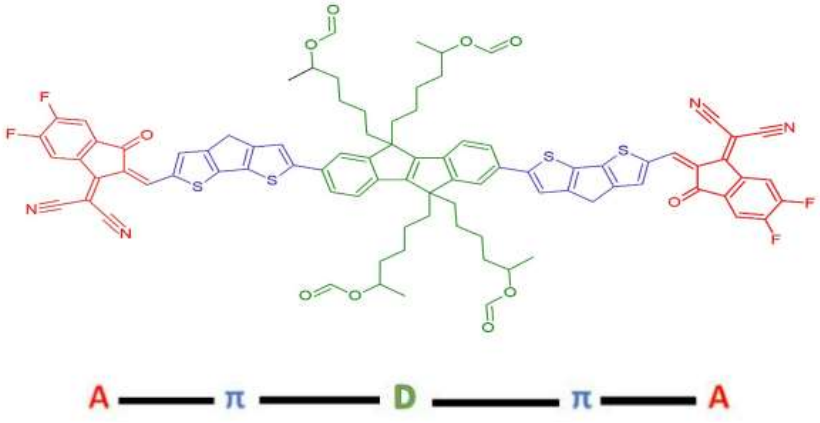


**Fig. 1.** Molecular configuration of the IDTIC-4F compound.

The main objective of the manuscript is to investigate the structural and optoelectronic properties of the non-fullerene acceptor IDIC-4F through computational methods. The study aims to provide insights into the electronic structure, charge transfer properties, and potential applications of IDIC-4F in organic solar cells. By analyzing the HOMO and LUMO energy levels, energy gap, and electron distribution within the molecule, the researchers seek to contribute to the understanding of IDIC-4F's performance in photovoltaic devices. To accomplish this objective, we employed Density Functional Theory (DFT) and Time-Dependent Density Functional Theory (TD-DFT). The selection of the most appropriate method was determined by comparing the obtained results with experimental findings in the literature. Furthermore, we evaluated the potential of the IDTIC-4F compound as a donor molecule, using the fullerene compound PCBM and the fullerene derivative $PC_{61}BM$ as acceptors.

## COMPUTATIONAL DETAILS

Initially, all of the molecular structures analyzed were constructed using ChemDraw 7.0 [30]. These designs were then imported into Gauss View 5.1.8 [31], which was also used to show the results of Gaussian 09 [32] quantum chemical calculations. B3LYP/6-31G(d,p) [33] was chosen to determine the geometric structures and electronic properties of the recommended compounds following an in-depth investigation of the band gap ($E_g$) of the parent molecule IDTIC-4F using the density functional method (DFT). Furthermore, the GaussSum software [34] was used to calculate density of states (DOS), and the Multiwfn 3.8 program [35] was used to generate transition density matrices (TDM) and charge density difference (CDD) maps.

Furthermore, the B3LYP/6-31G(d,p) approach was utilized to simulate UV-Vis absorption spectra in solvent (THF) with the IEF-PCM model (Integral Equation Formalism Polarizable Continuum Model) [36]. The correctness of the IEF-PCM model has been confirmed in the existing literature, as it concentrates on weak interactions such as hydrogen bonding and van der Waals forces, which are relevant to our molecular systems [37]. It is worth noting that remarkable NLO characteristics can have an effect on short-circuit current density. Equations (1) and (2) used B3LYP functionals with 6-31G(d,p) to calculate polarizability (α) and hyperpolarizability (β).

$$\alpha = \frac{1}{3}\left(\alpha_{xx} + \alpha_{yy} + \alpha_{zz}\right) \quad (1)$$

$$\beta = \sqrt{(\beta_{xxx} + \beta_{xyy} + \beta_{xzz})^2 + (\beta_{yyy} + \beta_{yxx} + \beta_{yzz})^2 + (\beta_{zzz} + \beta_{zxx} + \beta_{zyy})^2} \quad (2)$$

## RESULTS AND DISCUSSION

### Electronic Properties

The bandgap energy ($E_{gap}$ = $E_{LUMO}$ - $E_{HOMO}$) is principally responsible for electronic characteristics, as demonstrated by various previous studies [38-40]. To correctly duplicate the experimentally discovered electronic characteristics of IDTIC-4F, several DFT functionals must be used, followed by a comparison of theoretical and experimental results. It is crucial to note that DFT calculations assume the IDTIC-4F molecule is in an isolated form, which may affect the HOMO and LUMO levels in solution. Table 1 shows the HOMO and LUMO energy levels, as well as the $E_{gap}$ of the IDTIC-4F molecule, as estimated using various functionals. The values obtained for the B3LYP/6-31G(d,p), B3LYP/6-311G(d,p), B3PW91/6-311G(d,p), and MPW1PW91/6-311G(d,p) methods are (-5.254, -3.295, 1.959 eV), (-5.495, -3.530, 1.965 eV), (-5.577, -3.597, 1.980 eV), and (-5.676, -3.451, 2.225 eV), respectively. The computed energy gaps range between 1.959 eV and 2.225 eV. When these findings are compared to experimental values (-5.680, -3.800, 1.880 eV), we can see that the B3LYP functional with 6-31G(d,p) base gives comparable results with a fair margin of error (Fig. 2). The observed disparity is mostly due to the assumptions employed in the DFT calculations, which assume the chemical under investigation as being in a gaseous form. As a result, it can be concluded that the B3LYP function with a base of 6-31G(d,p) is particularly well-suited for defining the electrical characteristics of the examined molecule [41].

**Table 1.** The Calculated Values of the HOMO and LUMO Energy Levels and the Gap Energy $E_{gap}$ Obtained by the B3LYP/6-31G(d,p), B3LYP/6-311G(d,p), B3PW91/6-311G(d,p), and MPW1PW91/6-311G(d,p) Methods

| Methods | $E_{HOMO}$ (eV) | $E_{LUMO}$ (eV) | $E_{gap}$ (eV) | μ (Debye) |
|---|---|---|---|---|
| B3LYP/6-31G(d,p) | -5.254 | -3.295 | 1.959 | 7.045 |
| B3LYP/6-311G(d,p) | -5.495 | -3.530 | 1.965 | 6.922 |
| B3PW91/6-311G(d,p) | -5.577 | -3.597 | 1.980 | 7.023 |
| MPW1PW91/6-311G(d,p) | -5.676 | -3.451 | 2.225 | 6.940 |
| Exp. [29] | -5.680 | -3.800 | 1.880 | - |

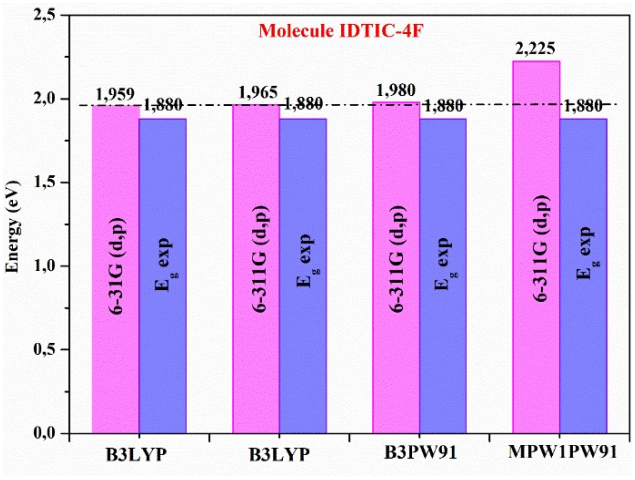


**Fig. 2.** The experimentally determined gap energy (E_gap) of the IDTIC-4F compound was compared to values calculated using DFT/6-31G(d,p) and 6-311G(d,p) at various functional levels.

## Geometrical Parameters

The geometrical properties of the IDTIC-4F compound were ascertained by extensively optimizing its structure in the ground state. This optimization was performed using several methods, including B3LYP/6-31G(d,p) [42], B3LYP/6-311G(d,p), B3PW91/6-311G(d,p) [31], and MPW1PW91/6-311G(d,p) [43]. Figure 3 depicts the bond lengths and dihedral angles in the IDTIC-4F complex. In Fig. 4, the optimal geometry obtained through the B3LYP/6-31G(d,p) technique is depicted. The corresponding bond lengths and dihedral angles, presented in Table 2, were calculated using various methods. According to Table 2, The bond lengths ($d_1$ and $d_2$) computed using methods B3LYP/6-31G(d,p), B3LYP/6-311G(d,p), B3PW91/6-311G(d,p), and MPW1PW91/6-311G(d,p) are (1.39, 1.41 Å), (1.38, 1.41 Å), (1.38, 1.41 Å), and (1.38, 1.41 Å), respectively. Another set of bond lengths ($d_3$; $d_4$; $d_5$; $d_6$) are (1.46, 1.46, 1.41, 1.38 Å), (1.46, 1.46, 1.41, 1.38 Å), (1.46, 1.46, 1.41, 1.38 Å), and (1.46, 1.46, 1.41, 1.38 Å), varying between 1.38 Å and 1.46 Å, indicating the nature of C = C and C - C bonds based on the results obtained. Dihedral angles θi (i = 1-6) range from 180° to 154°, confirming a planar conformation that enhances conjugation. Specifically, $\theta_1$, $\theta_2$, $\theta_5$, and $\theta_6$ are close to 180° due to minimal deviation from the plane, whereas $\theta_3$ and $\theta_4$ range between 157.04° and 153.94°, influenced by intermolecular forces. The bond lengths di (i = 1-6) closely approximate 1.4 Å, underscoring the molecule's highly planar structure and promoting π–π* interactions to facilitate charge carrier mobility [44].

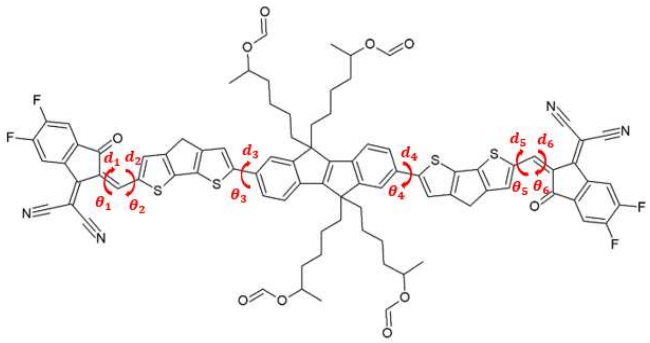


**Fig. 3.** Chemical structure of the IDTIC-4F compound showing the positions of the bond lengths $d_i$ and the dihedral angles $\theta_i$.

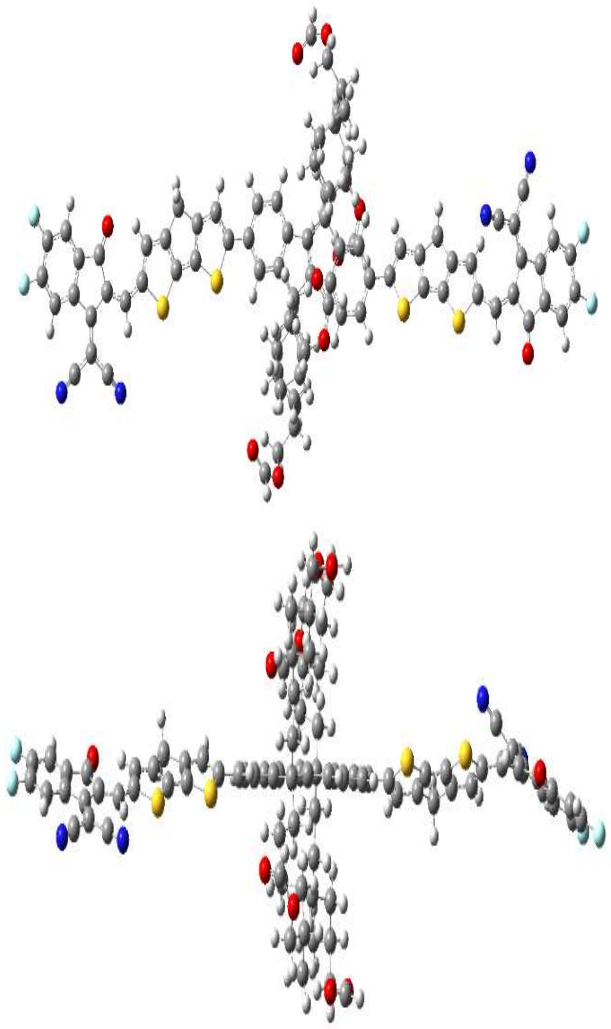

**Fig. 4.** Optimized structure of the IDTIC-4F compound obtained by B3LYP/6-31G(d,p) method.

## Optical Properties

Several evaluations were carried out using various quantum chemistry approaches to determine the best quantum method for understanding the effect of excitation and electronic transitions in the IDTIC-4F molecule. The optimized geometries were created using the following methods: TD-DFT/B3LYP/6-31G(d,p), B3PW91/6-31G(d,p), CAM-B3LYP/6-31G(d,p), MPW1PW91/6-31G(d,p), and WB97XD/6-31G(d,p). Table 3 summarizes the parameters for absorption wavelengths ($\lambda_{max}$), oscillator strengths (f), vertical excitation energies, and experimental absorption data from IDTIC-4F spectra. Table 3 shows that the maximum absorption values ($\lambda_{max}$) calculated by TD-DFT/B3LYP/6-31G(d,p), B3PW91/6-31G(d,p), CAM-B3LYP/6-31G(d,p), MPW1PW91/6-31G(d,p), and WB97XD/6-31G(d,p) methods are (712.01, 710.40, 552.04, 670.55, 534.460 nm), while the experimental value in THF solvent was 715 nm. As a consequence, TD-B3LYP/6-31G(d,p) was chosen for additional electrical simulations because of its close agreement with the literature-reported max value (711 nm). These results lend credence to the TD-B3LYP/6-31G(d,p) technique for assessing the IDTIC-4F molecule's absorption characteristics. The observed first transition has a low transition energy and a high oscillation factor, followed by a secondary transition with a low oscillation factor. The most common transition from the ground state to the excited state is the p-p* transition, which occurs between the highest occupied molecular orbital (HOMO) p and the lowest unoccupied molecular orbital

**Table 2.** Geometric Parameters (Bond Lengths $d_i$(Å), Dihedral Angles $\theta_i$(º)) of the Optimized Structure of the IDTIC-4F Compound Obtained at Different Theoretical Levels

| Methods | Bond lengths $d_i$ (Å) | | | | | | Dihedral angles $\theta_i$ (º) | | | | | |
|---|---|---|---|---|---|---|---|---|---|---|---|---|
| | $d_1$ | $d_2$ | $d_3$ | $d_4$ | $d_5$ | $d_6$ | $\theta_1$ | $\theta_2$ | $\theta_3$ | $\theta_4$ | $\theta_5$ | $\theta_6$ |
| B3LYP/6-31G(d,p) | 1.39 | 1.41 | 1.46 | 1.46 | 1.41 | 1.38 | -179.73 | -179.73 | 156.15 | 157.04 | -175.23 | -172.47 |
| B3LYP/6-311G(d,p) | 1.38 | 1.41 | 1.46 | 1.46 | 1.41 | 1.38 | -179.58 | -179.73 | 154.98 | 154.93 | -162.04 | -172.32 |
| B3PW91/6-311G(d,p) | 1.38 | 1.41 | 1.46 | 1.46 | 1.41 | 1.38 | -179.47 | -179.69 | 155.46 | 154.22 | -175.21 | -172.35 |
| MPW1PW91/6-311G(d,p) | 1.38 | 1.41 | 1.46 | 1.46 | 1.41 | 1.38 | -179.67 | -179.79 | 154.35 | 153.94 | -174.79 | -172.56 |

**Table 3.** Values of Absorption Length, Oscillator Strengths, Excitation Energy, and the Transition Character in the UV-visible Area of the IDTIC-4F Compound were Calculated at the TD-DFT Level in the Solvent Phase (THF)

| Methods | Energy (eV) | Wavelength (nm) | Osc. Strength *f* | MO/Character |
|---|---|---|---|---|
| B3LYP/6-31G(d,p) | 1.728 | 712.01 | 2.275 | H→ L (0.69) |
| | 1.897 | 649.25 | 0.372 | H → L+1 (0.69) |
| | 2.156 | 565.94 | 0.130 | H-1→ L (0.68) |
| B3PW91/6-31G(d,p) | 1.726 | 710.40 | 2.266 | H→ L (0.69) |
| | 1.845 | 645.19 | 0.360 | H → L+1 (0.68) |
| | 2.120 | 562.29 | 0.128 | H-1→ L (0.68) |
| CAM-B3LYP/6-31G(d,p) | 2.198 | 552.04 | 3.763 | H → L (0.47) |
| | 2.421 | 510.16 | 0.211 | H → L+1 (0.47) |
| | 3.061 | 400.32 | 0.345 | H → L+2 (0.38) |
| MPW1PW91/6-31G(d,p) | 1.712 | 670.55 | 2.731 | H → L (0.66) |
| | 2.031 | 608.61 | 0.280 | H → L+1 (0.68) |
| | 2.289 | 530.55 | 0.090 | H-1→ L (0.68) |
| WB97XD/6-31G(d,p) | 2.306 | 534.60 | 3.740 | H → L (0.43) |
| | 2.498 | 497.39 | 0.261 | H → L+1 (0.43) |
| | 3.189 | 389.34 | 0.451 | H → L+2 (0.38) |
| Exp. [29] | - | 715 | - | - |

(LUMO) p*. Figure 5 shows the UV-visible absorption spectra of the IDTIC-4F compound as simulated using several TD/DFT techniques, with TD-B3LYP/6-31G(d,p) demonstrating significant, wide absorption in the visible region (400-800 nm) and a peak at 712.01 nm.

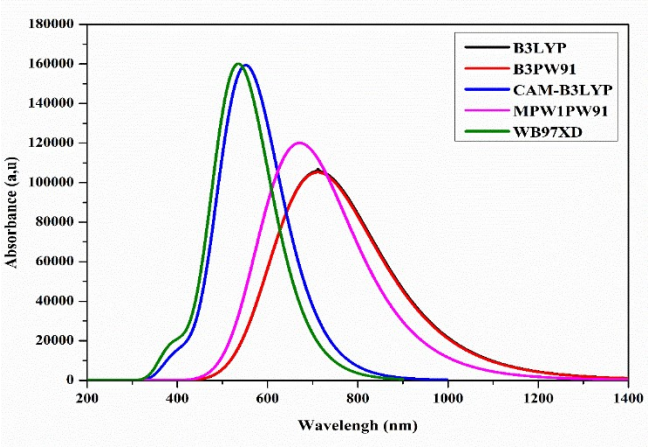


**Fig. 5.** Study of the spectra of molecule IDTIC-4F with three various functionals in solvent phase (THF).

The nonlinear absorbance (NLO) characteristics of molecules are critical in optoelectronic applications [45]. Indeed, delocalized intramolecular charge influences the nonlinear optical (NLO) characteristics of organic molecules, allowing for efficient charge separation between donor (D) and acceptor (A) units. The π-conjugated bridges increase electron mobility and optimize energy levels, which improves light absorption and charge transfer. A greater Intramolecular Charge Transfer (ICT) value correlates with a larger NLO [46]. As a result, NLO characteristics may be utilized to explain the electronic charge transport efficiency of organic compounds, which influences saturation current ($J_{sc}$) and energy conversion efficiency (PCE). Table 4 displays the determined NLO parameters of the IDTIC-4F molecule, including polarizability (α) and first-order hyperpolarizability (β). Table 4 shows that IDTIC-4F has a higher electronic charge transfer efficiency ($\alpha$ = 1910.973 a.u). Concerning β, IDTIC-4F has a value of 35499.620 a.u, indicates better photocurrent responsiveness and effectiveness due to its substantial NLO features [47].

**Table 4.** The Values of Calculated Polarizability (α), and First-order Hyperpolarizability (β) of the IDTIC-4F Compound

| Parameters | IDTIC-4F |
|---|---|
| Polarizability (a.u) | |
| $\alpha_{xx}$ | 3875.584 |
| $\alpha_{yy}$ | 1134.906 |
| $\alpha_{zz}$ | 722.429 |
| $\alpha_{tot}$ | 1910.973 |
| Hyperpolarizability (a.u) | |
| $\beta_{xxx}$ | 25581.202 |
| $\beta_{xxy}$ | -24129.159 |
| $\beta_{xyy}$ | -607.049 |
| $\beta_{yyy}$ | -224.295 |
| $\beta_{xxz}$ | 6683.538 |
| $\beta_{xyz}$ | -721.248 |
| $\beta_{yyz}$ | -22.689 |
| $\beta_{xzz}$ | 25.753 |
| $\beta_{yzz}$ | 46.435 |
| $\beta_{zzz}$ | 2.227 |
| $\beta_{tot}$ | 35499.620 |

## Frontier Molecular Orbitals (FMO)

Understanding a molecule's Frontier Molecular Orbitals (FMO) is essential for studying its optoelectronic capabilities since it reveals the distribution of charge density across the molecule. When electrons in a molecule are exposed to light of a specific wavelength, they move from the ground state (HOMO) to the excited state (LUMO). The energy difference between these states, known as the band gap (HOMO-LUMO), is essential [48-51]. Figure 6 shows the HOMO and LUMO configurations of the IDTIC-4F molecule, showing an acceptor-bridge-donor-bridge-acceptor (A-π-D-π-A) structure with acceptor malononitrile connected to the donor compound's indenoindene group. The electron-drawing acceptor groups at the terminal, which start with the indenoindene donor core and work their way up to the malononitrile acceptor groups, induce charge mobility. This process allows for significant charge delocalization on the IDTIC-4F *via* conjugation, which is facilitated by the compound's rigid, planar structure. The HOMO has a concentrated charge density in the indenoindene group, whereas the LUMO has a distributed charge density, mostly in the malononitrile acceptor groups.

Due to its relatively flat structure, the HOMO distribution is primarily located in the indenoindene donor group [52]. Conversely, the LUMO distribution in the acceptor (malononitrile) is less spatially overlapping, enhancing the electronic coupling between the acceptor and donor units. This results in a greater driving force for charge transfer and reduced recombination losses. The red and green FMO lobes represent the positive and negative phases, respectively [53]. The findings on FMO spatial delocalization and energy level alignment suggest that the acceptor has efficient charge extraction and transport capabilities, higher conductivity, and a reduced likelihood of current loss due to recombination. The analyzed molecular charge distribution pattern demonstrates excellent charge transfer capabilities, which are essential for the development of improved Organic Solar Cells (OSCs).

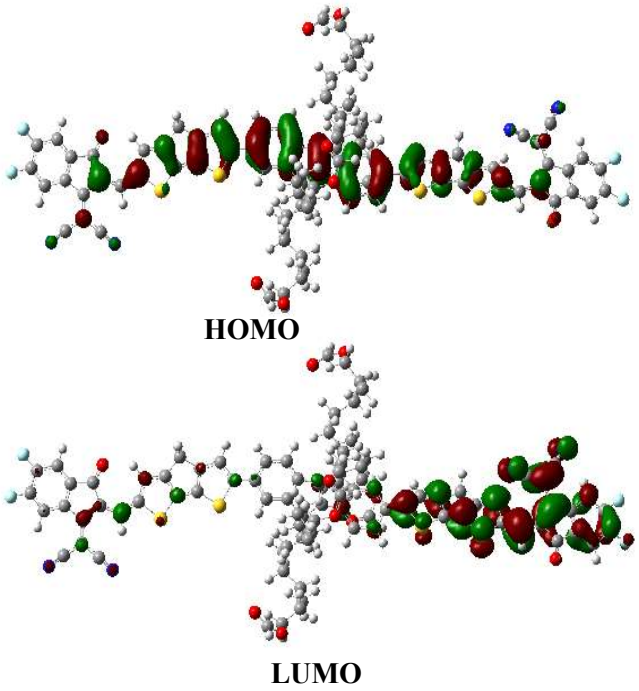


**Fig. 6.** Frontier molecular orbital of IDTIC-4F compound at B3LYP/6-31G(d,p) level.

## Molecular Electrostatic Potential Surface (MEPS)

Molecular electrostatic potential (MEP) surface maps illustrate the spatial arrangement of positive and negative charges across a molecular system. These MEP surfaces employ a color scale, with red indicating highly negative potential and blue representing positive electrostatic potential. The 3D surface analysis evaluates molecule segments based on their sensitivity to electrophilic or nucleophilic attacks. A red zone signifies a favorable site for electrophilic attack, whereas a blue region indicates sensitivity to nucleophilic attack [54,55].

Figure 7 shows the visual analysis of the IDTIC-4F compound using Density Functional Theory (DFT) at the B3LYP/6-31G(d,p) level of theory. The red and orange hues of the cyano groups in acceptors indicate a high electron density in the studied molecule, implying that dicyanide groups are loosely connected and particularly vulnerable to electrophilic attacks. Furthermore, the oxygen atom in the acceptor groups exhibits a red cloud, indicating a high electron density. Nitrogen atoms within the donor core have positive electron density, as seen by a slightly blue cloud in their proximity. Nitrogen's natural electron density is counteracted by electrically deficient adjacent acceptors, resulting in the formation of a positive electrostatic potential and making it a reactive nucleophilic site. In conclusion, the IDTIC-4F compound's remarkable charge transfer to excitation, which is linked to electron density occupancy in distinct locations, places it as a possible candidate for effective future photovoltaic solar cells (PSCs).

.

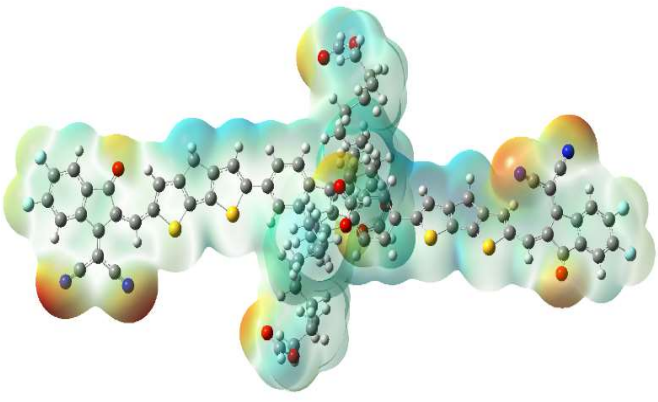

**Fig. 7.** MEP plots of IDTIC-4F compound at B3LYP/6-31G(d,p) level.

## Density of State (DOS) Analysis

The electronic load transmission between distinct fragments within an organic system is examined using DOS analysis to validate FMO survey results [56]. This questionnaire is widely used to determine the percentage contribution of each unit in a compound to the overall distribution of electronic load [57,58]. As a result, the IDTIC-4F compound studied is separated into three segments for the analysis of their DOS map: (i) the central donor, (ii) the bridge, iii) cap terminal acceptors (A). Each chromophore unit is denoted by a distinct color, with donor represented in bleu, π-spacing represented in vert, while the peripheral acceptors are depicted in pink, as shown in the DOS pictograms in Fig. 8. For IDTIC-4F, the DOS results reveal that in the current survey, the donor accounts for 44% of the electronic contribution to HOMO, whereas 6% is distributed to LUMO, while the distribution model presented by bridge is 39% for HOMO and 34% for LUMO. Additionally, the distribution model presented by terminal acceptors is 14% for HOMO and 60% for LUMO in the IDTIC-4F chromophore.

According to Fig. 8, the maximum intensity of the blue peak suggests that the HOMO load density is largely concentrated above the donor region of IDTIC-4F. In contrast, the pink peak shows that the acceptor has the highest load distribution compared to LUMO. In conclusion, the examined chromophore DOS spectrum (IDTIC-4F) shows a considerable load transfer from HOMO to LUMO, indicating that it is a good candidate for non-fullerene organic solar cells. According to the results (Fig. 8), HOMO density is predominantly found in the donor benzodithiophene group, whereas LUMO density is generally found in the accepting section. The donor entity of the compound investigated has the highest HOMO density, whereas the acceptor unit has the lowest vacant compound orbital.

## TDM (Transition Density Matrix) Analysis

Analyzing electronic excitation phenomena between distinct molecular fragments is effectively achieved through the use of TDM analysis. This research contributes to understanding the quantum geometry of model IDTIC-4F through excitation measurements. TDM analysis was performed on the compounds of interest using a 6-31G(d,p) basis and the selected hybrid functional (B3LYP). The obtained data was then processed with the Multiwfn 3.7 software.

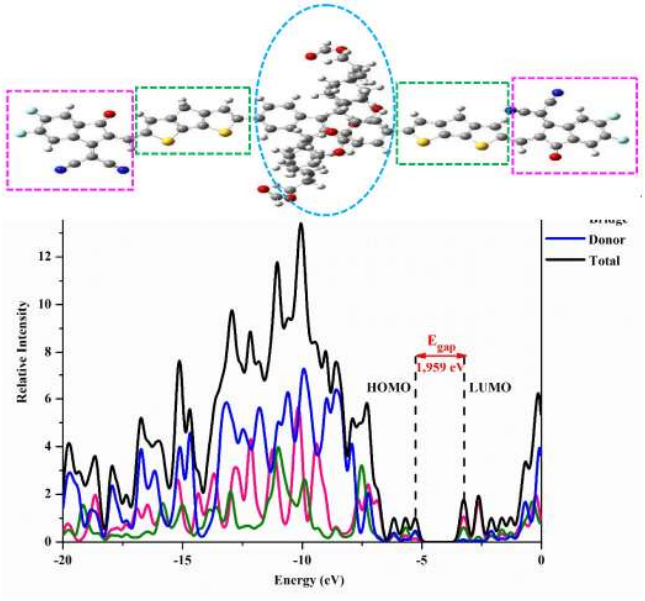


**Fig. 8.** Density of state (DOS) plots of the IDTIC-4F at B3LYP/6-31G(d,p) level.

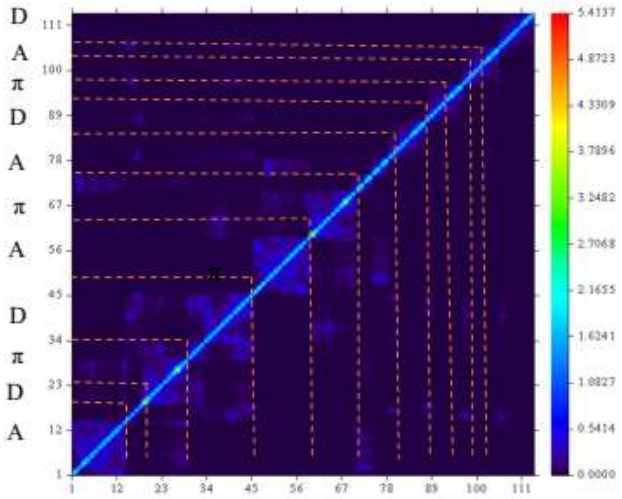


**Fig. 9.** TDM plots of the IDTIC-4F at B3LYP/6-31G(d,p) level.

The electronic charge density is shown in the TDM maps with different hues, extending across the spectrum from blue to red, the bright spots in the figures signify notable charge mobilities originating from the donor moiety and moving towards the acceptor subunit. The electronic charge density increases from bottom to top on the right side of the vertical axis, because hydrogen atoms have limited significance in the excitation process, they are ignored in the TDM graphs. The bright edges of the TDM map analysis reflect the fraction of fermions and transition states controlling the excitation event [59,60]. In TDM graphs, a blue color implies lesser charge density, whereas a red tint shows higher charge density. Green, cyan, and yellow represent intermediate electrical densities [61]. Figure 9 depicts a visual depiction of TDM research using the model IDTIC-4F. Diagonal and off-diagonal charge transfer signifies a low electron coupling, facilitating swift electron dissociation necessary for the optimal performance of organic solar cells (OSCs). In the TDM analysis, charge localization is visually shown by dark spikes [62].

## Educed Density Gradient (RDG) Exploration

The reduced density gradient (RDG) s examined to determine the presence of non-covalent interactions (NCIs) caused by interacting forces inside molecules (O—S, O—H, F—H, and N—S). RDG is useful in studying several NCIs, including hydrogen bonding, London dispersion forces (LDF), Van der Waals forces, and steric hindrance. These interactions are critical in inhibiting molecular self-assembly, guaranteeing tight packing in the molecular structure, limiting free rotation around single bonds, increasing charge transfer, and promoting crystallinity [49]. These strategies dramatically improve the optoelectronic characteristics of molecules. Non-covalent interactions (NCIs) are shown using VMD 1.9 and Multiwfn 3.8 software. Positive sign ($\lambda_2$) values reflect strong repulsive interactions in red saturation. Green color concentration is a main signal of attracting forces such as LDF, whereas blue colors indicate the presence of hydrogen bonds. These interactions are critical for determining molecular stability and promoting charge transfer. In the color spectrum, green saturation implies hydrogen bonding between extremely electronegative oxygen atoms and strongly electropositive hydrogen atoms, whereas blue saturation relates to electronegative elements such as fluorine, oxygen, and sulfur. Comparable structures, such as five- and six-membered rings, exhibit repulsive forces (Fig. 10). All of these interactions help to create planarity in the molecular structure, which facilitates efficient charge transfer. These results improve our

understanding of the molecular principles underpinning organic solar cells, which aids in their optimization and progress.

## Electron Density Difference Maps

Examining electron density difference maps (EDDM) between excited and ground states helps us better comprehend exciton separation in the excited state and subsequent charge separation [50]. The EDDM maps (Fig. 11) show a charge transfer between the excited and ground states in the instance of compound IDTIC-4F under investigation. The flow of electrical charges from the donor (indenoindene core) to the malononitrile terminal *via* the cyclopentadithiophene bridge is what causes this dynamic. According to EDDM, the decrease in electron density (in blue) is mostly caused by the indenoindene group (as donor), .

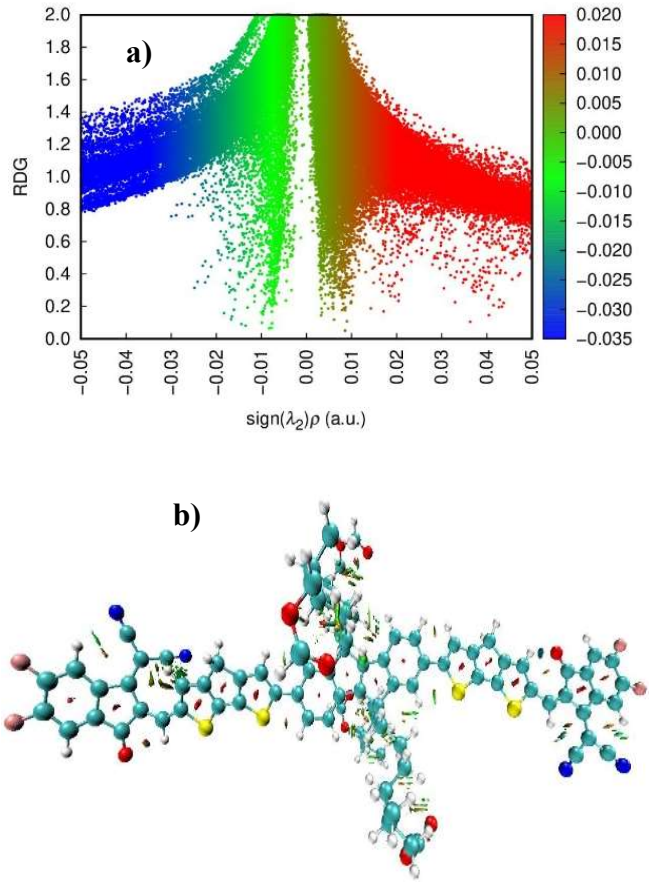


**Fig. 10.** a) Scatter graphs and b) gradient isosurfaces of IDTIC-4F molecule.

with the spacer contributing minimally. For the chemical IDTIC-4F, the area of increased electron density (shown in purple) is concentrated on the acceptor, with little participation from the spacer. These results imply that in this compound IDTIC-4F, an intramolecular charge transfer between the HOMO and LUMO orbitals occurs, resulting in a reduction in the band gap and a shift in absorption to the red region, which is crucial for the efficiency of organic solar cells.

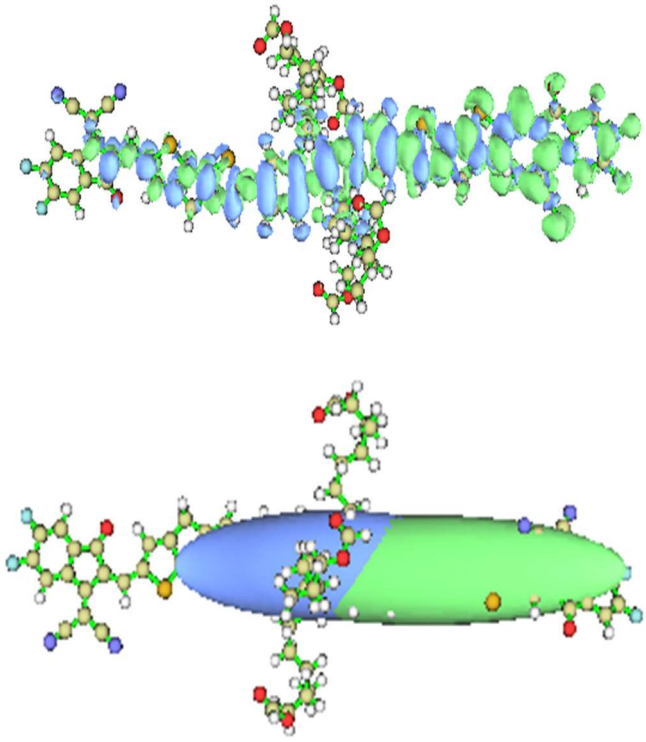

**Fig. 11.** Electron density difference maps between the excited states and the ground ones of the compound IDTIC-4F.

## Quantum Chemical Parameters

To assess the chemical reactivity and kinetic stability of the recently synthesized molecule, diverse chemical parameters were computed, and the outcomes are presented in Table 5 and Fig. 12. The calculation of the chemical potential was carried out using Eq. (3) [51].

$$\mu = \frac{(E_{HOMO}+E_{LUMO})}{2} \quad (3)$$

**Table 5.** Calculated $E_{HOMO}$, $E_{LUMO}$, Hardness (η), Chemical Potential (μ), Electronegativity (**χ**), Electrophilicity Index (**ω**) Values of the Studied Compounds

| Compounds | $E_{HOMO}$ (eV) | $E_{LUMO}$ (eV) | μ (eV) | η (eV) | **χ** (eV) | **ω** (eV) |
|---|---|---|---|---|---|---|
| IDTIC-4F | -5.254 | -3.295 | -4.274 | 0.979 | 4.274 | 9.329 |
| **$PC_{61}BM$** | -6.100 | -3.700 | -4.900 | 1.200 | 4.900 | 10.000 |
| **$PC_{71}BM$** | -5.960 | -3.900 | -4.930 | 1.030 | 4.930 | 11.798 |
| **$C_{60}$** | -5.900 | -4.200 | -5.050 | 0.850 | 5.050 | 15.001 |

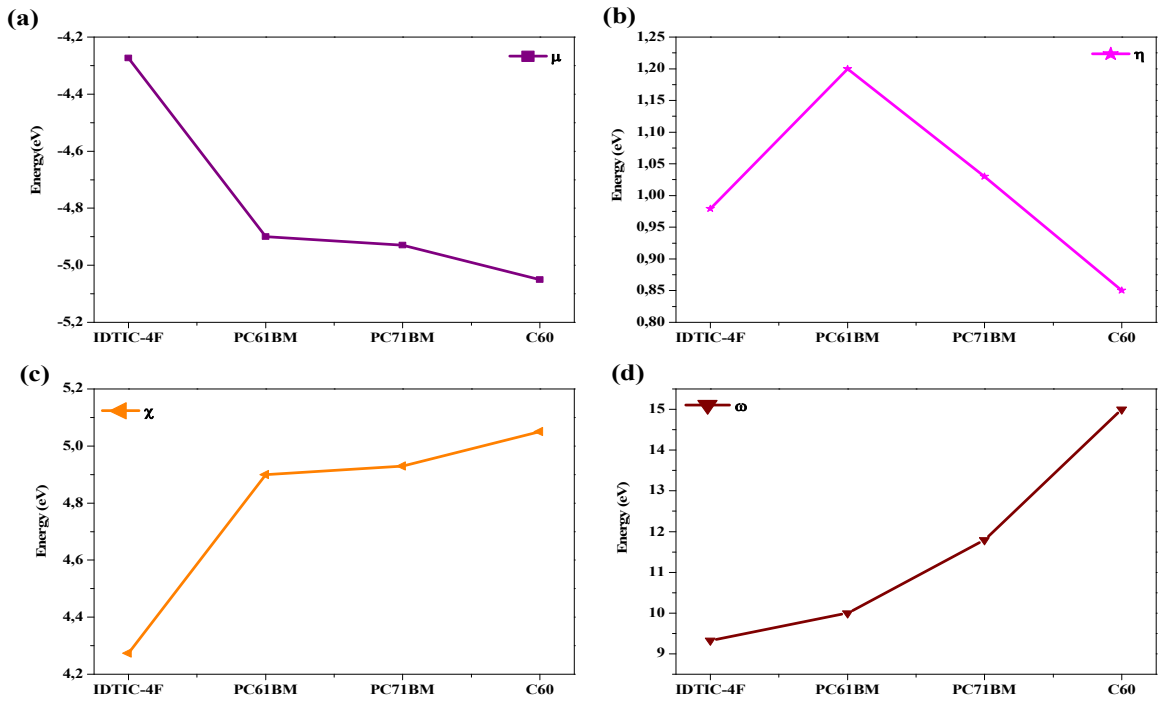


**Fig. 12.** (a) Chemical potential (μ), (b) chemical hardness (η), (c) electron negativity (χ), and (d) electrophilicity index (ω) for IDTIC-4F compound calculated at B3LYP/6-31G(d,p) level.

The chemical potential characterizes the electron cloud's ability to disperse. In comparison to $PC_{61}BM$, $PC_{71}BM$ and $C_{60}$, the IDTIC-4F molecule exhibits a higher chemical potential value, signifying its superior capability to donate electrons.

$$\eta = \frac{(E_{LUMO} - E_{HOMO})}{2} \quad (4)$$

Computed *via* Eq. (4) [52], the chemical hardness values indicate that the IDTIC-4F molecule is categorized as soft, characterized by reduced band gaps and heightened chemical reactivity.

$$\boldsymbol{\omega} = \frac{\mu^2}{2\eta} \quad (5)$$

$$\chi = -\mu = -\frac{(E_{HOMO}+E_{LUMO})}{2} \quad (6)$$

Using Eqs. (5) and (6) [53,63], we simulated the electrophilicity index and electron negativity values, respectively. These two parameters are commonly interrelated and offer a quantitative description of the electronic characteristics of molecules. In comparison to $PC_{61}BM$, $PC_{71}BM$ and $C_{60}$, IDTIC-4F displays lower electronegativity and electrophilicity index values, suggesting its diminished capacity to attract electrons from the acceptors and function as an electron donor (Fig. 12).

## Photovoltaic Properties

To study the photovoltaic properties (fullerene derivatives), the ability of electron transfer from the IDTIC-4F compound to the conducting band of the acceptor compounds (Fig. 13) must be investigated. To allow for efficient exciton dissociation, the energy level of the donor's LUMO appears to be at least 0.3 eV higher than that of the acceptor's LUMO [35]. a represents the difference between IDTIC-4F's and the acceptor's LUMOs:

$$\alpha = E_{LUMO}(IDTIC-4F) - E_{LUMO}(Acceptor) \quad (7)$$

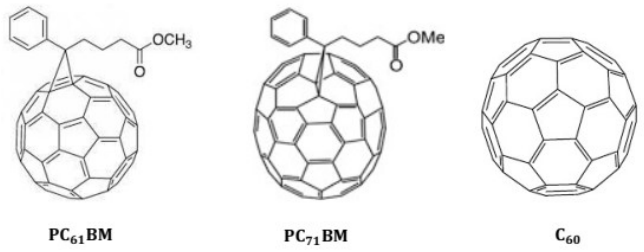


**Fig. 13.** Chemical structures of $PC_{61}BM$, $PC_{71}BM$ and $C_{60}$ acceptors.

Figure 14 shows the HOMO and LUMO energy levels of the IDTIC-4F molecule with several acceptors. The obtained energy map shows that the LUMO level of IDTIC-4F surpasses that of acceptors such as $PC_{61}BM$, $PC_{71}BM$, and $C_{60}$, with energy differences of 0.268, 0.468, 0.568, and 0.768 eV, respectively, as shown in Table 6. This discrepancy implies the possibility of electron transfer from the IDTIC-4F compound to the conduction band of the matching acceptor molecules.

The open-circuit voltage ($V_{oc}$), which represents the maximum voltage obtainable in a heterojunction-type open circuit, is one component that influences solar cell efficiency. $V_{oc}$ is defined as the difference between the HOMO of the electron donor and the LUMO of the electron acceptor, taking into account the energy lost during photocharge creation [64,65].

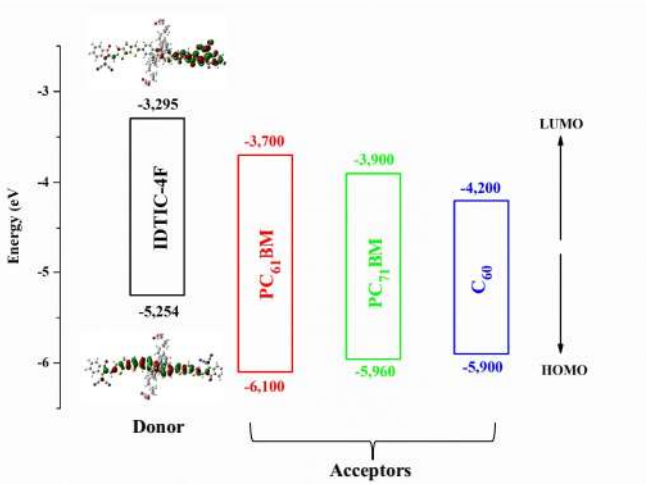


**Fig. 14.** The HOMO and LUMO energy levels of IDTIC-4F compound and the acceptors.

**Table 6.** The Values of $E_{HOMO}$, $E_{LUMO}$, $\alpha = E_{LUMO}^{Donor} - E_{LUMO}^{Acceptor}$ and the Open-circuit Voltage ($V_{oc}$) in (V) of the Donor, IDTIC-4F, with Different Acceptors

| Molecules | $E_{HOMO}$ (eV) | $E_{LUMO}$ (eV) | R/**$PC_{61}BM$** | | R/**$PC_{71}BM$** | | R/**$C_{60}$** | |
|---|---|---|---|---|---|---|---|---|
| | | | $V_{oc}$ (V) | α | $V_{oc}$ (V) | α | $V_{oc}$ (V) | α |
| IDTIC-4F | -5.254 | -3.295 | 1.254 | 0.405 | 1.054 | 0.605 | 0.754 | 0.905 |
| **$PC_{61}BM$** | -6.100 | -3.700 | - | - | - | - | - | - |
| **$PC_{71}BM$** | -5.960 | -3.900 | - | - | - | - | - | - |
| **$C_{60}$** | -5.900 | -4.200 | - | - | - | - | - | - |

The following empirical equation [66] expresses the $V_{oc}$:

$$V_{oc} = \frac{1}{e}(|E_{HOMO}(D) - E_{LUMO}(A)|) - 0.3 \quad (8)$$

Table 6 presents the energy levels $E_{LUMO}$, $E_{HOMO}$, $V_{oc}$ (open-circuit voltage), and $\alpha = E_{LUMO}^{Donor} - E_{LUMO}^{Acceptor}$. The $V_{oc}$ values obtained from the IDTIC-4F compound combined with various acceptors are detailed in the table, ranging from 0.754 to 1.254 V. These values indicate sufficient voltage for effective electron injection into the cell. Notably, the highest $V_{oc}$ value (1.254 V) is achieved when utilizing the $PC_{61}BM$ acceptor, which exhibits a minimal energy difference ($\alpha = E_{LUMO}^{IDTIC-4F} - E_{LUMO}^{PC61BM} = 0.3$ eV), consistent with previous findings [67].

Furthermore, an energy difference greater than this minimum value between the donor and acceptor LUMOs results in energy loss during exciton separation, which has a negative impact on device performance [68]. This finding is consistent with the table results, which demonstrate a decrease in $V_{oc}$ and an increase in LUMO energies between the donor and acceptor. This study demonstrates that the IDIC compound functions effectively as an electron donor material with the tested acceptors, ensuring a constant injection of electrons from the donor into the acceptors' conduction band.

## CONCLUSION

In this study, we used several functionals from the Density Functional Theory (DFT) technique to theoretically compute the structural, optical, and electrical characteristics of the IDTIC-4F compound. A. Zulfiqar and coworkers [29] created the IDTIC-4F molecule, which functions as an acceptor material. The fundamental goals of this work were twofold: first, to determine the most appropriate DFT and TD-DFT functionals that corresponded to experimental data, and second, to assess the IDTIC-4F molecule as an electron donor in combination with several fullerene derivatives as acceptors.

The results showed that the DFT/B3LYP/6-31G(d,p) level predicted the molecule's electrical and optical characteristics with great precision. At this level, the IDTIC-4F compound has a gap energy of 1.959 eV, diffuse visible light absorption from 500 to 900 nm, and a clear absorption peak at 712.01 nm in its isolated state. When the studied compound was coupled with $PC_{61}BM$, $PC_{71}BM$ and $C_{60}$ as an acceptor, the predicted open-circuit voltage ($V_{oc}$) values ranged from 0.754 to 1.254 V. The $PC_{61}BM$ acceptor had the greatest $V_{oc}$ value, indicating the substantial potential for effective electron injection from IDTIC-4F as a donor into the acceptors' conduction bands. When evaluated against several parameters, the IDTIC-4F molecule emerges as a potential option for organic solar cells, performing the role of a combined electron donor with the $PC_{61}BM$ fullerene acting as the acceptor.

## REFERENCE

[1] Coyle, E. D; Simmons, R. A., Understanding the global energy crisis. *Purdue Univ. Press.* **2014**, http://library.oapen.org/handle/20.500.12657/30124.

[2] Sadorsky, P., The effect of urbanization and industrialization on energy use in emerging economies: implications for sustainable development. *Am. J. Econ. Sociol.* **2014**, *73*, 392-409. DOI: 10.1111/ajes.12072.

[3] Waheed, R.; Sarwar, S.; Wei, C., The survey of economic growth, energy consumption and carbon emission. *Energy Rep.* **2019**, *5*, 1103-1115. DOI: 10.1016/ j.egyr.2019.07.006.

[4] Malanima, P., Energy crisis and growth 1650-1850: the European deviation in a comparative perspective. *J. Glob. Hist.* **2006**, *1*, 101-121. DOI: 10.1017/ S1740022806000064.

[5] Abas, N.; Kalair, A.; Khan, N., Review of fossil fuels and future energy technologies. *Futures*, **2015**, *69*, 31-49, DOI: 10.1016/j.futures.2015.03.003.

[6] Panwar, N.; Kaushik, S.; Kothari, S., Role of renewable energy sources in environmental protection: A review. *Renew. Sustain. Energy Rev.* **2011**, *15*, 1513-1524, DOI: 10.1016/j.rser.2010.11.037.

[7] Kannan, N.; Vakeesan, D., Solar energy for future world: -A review. *Renew. Sustain. Energy Rev.* **2016**, *62*, 1092-1105, DOI: 10.1016/j.rser.2016.05.022.

[8] Gong, J.; Li, C.; Wasielewski, M. R., Advances in solar energy conversion. *Chem. Soc. Rev.* **2019**, *48*, 1862-1864, DOI: 10.1039/C9CS90020A.

[9] Foster, R.; Ghassemi, M.; Cota, A., Solar energy: renewable energy and the environment. *CRC Press.* **2009**.

[10] Fahrenbruch, A.; Bube, R., Fundamentals of solar cells: photovoltaic solar energy conversion. *Elsevier*, **2012**.

[11] Wright, M.; Uddin, A., Organic-inorganic hybrid solar cells: a comparative review. *Sol. Energy Mater. Sol. Cells*. **2012**, *07*, 87-111, DOI: 10.1016/ j.solmat.2012.07.006.

[12] Yousaf, I.; Khera, R.A.; Iqbal, J.; Gul, S.; Jabeen, S.; Ihsan, A.; Ayub, K., Isatin-derived non-fullerene acceptors for efficient organic solar cells. *Mater. Sci. Semicond. Process.* **2021**, *121*, 105345, DOI: 10.1016/j.mssp.2020.105345.

[13] Bloking, J. T.; Han, X.; Higgs, A. T.; Kastrop, J. P.; Pandey, L.; Norton, J. E.; Risko, C.; Chen, C. E.; Brédas, J. L.; McGehee, M. D.; Sellinger, A., Solution-processed organic solar cells with power conversion efficiencies of 2.5% using benzothiadiazole/imide-based acceptors. *Chem. Mater.* **2011**, *23*, 5484-5490, DOI: 10.1021/cm203111k.

[14] Scharber, M. C.; Sariciftci, N. S., Efficiency of bulk-heterojunction organic solar cells. *Prog. Polym. Sci.* **2013**, *38*, 1929-1940. DOI: 10.1016/ j.progpolymsci.2013.05.001.

[15] Chen, L. X., Organic Solar Cells: Recent Progress and Challenges. *ACS Publ.* **2019**, *4*, 2537-2539, DOI: 10.1021/acsenergylett.9b02071.

[16] Zhang, G.; Zhao, J.; Chow, P. C. Y.; Jiang, K.; Zhang, J.; Zhu, Z.; Zhang, J.; Huang, F.; Yan, H., Nonfullerene acceptor molecules for bulk heterojunction organic solar cells. *Chem. Rev.* **2018**, *118*, 3447-3507, DOI: 10.1021/acs.chemrev.7b00535.

[17] Vithanage, D. A.; Devižis, A.; Abramavičius, V.; Infahsaeng, Y.; Abramavičius, D.; MacKenzie, R. C. I.; Keivanidis, P. E.; Yartsev, A.; Hertel, D.; Nelson, J.; Sundström, V.; Gulbinas, V., Visualizing charge separation in bulk heterojunction organic solar cells. *Nat. Commun.* **2013**, *4* (1), 1-6, DOI: 10.1038/ncomms3334.

[18] Li, Y.; Yu, L.; Chen, L.; Han, C.; Jiang, H.; Liu, Z.; Zheng, N.; Wang, J.; Sun, M.; Yang, R.; Bao, X., Subtle side chain triggers unexpected two-channel charge transport property enabling 80% fill factors and efficient thick-film organic photovoltaics. *Innovation,* **2021**, *2*, 100090, http://creativecommons.org/licenses/by-nc-nd/4.0/.

[19] Chen, S.; Liu, Y.; Zhang, L.; Chow, P. C. Y.; Wang, Z.; Zhang, G.; Ma, W.; Yan, H., A wide-bandgap donor polymer for highly efficient non-fullerene organic solar cells with a small voltage loss. *J. Am. Chem. Soc.* **2017**, *139*, 6298-6301, DOI: 10.1021/jacs.7b01606.

[20] Mohajeri, A.; Kheshti, T., Improving the efficiency of dye-sensitized solar cells based on BODIPY dye and its analogous: The synergistic effect of benzo fusion and phenyl substitution. *J. Photochem. Photobiol. A: Chem.* **2023**, *442*, 114781, DOI: 10.1016/ j.jphotochem.2023.114781.

[21] Mohajeri, A.; Farmani, M., Toward More Efficient Organic Semiconductors: The Relationship between Morphology, Charge Transport, and Photophysical Properties. *ACS Appl. Electron. Mater.* **2022**, *4*, 246-258, DOI: 10.1021/acsaelm.1c00975.

[22] Mohajeri, A.; Omidvar, A., Fullerene-based materials for solar cell applications: design of novel acceptors for efficient polymer solar cells - a DFT study, *Phys. Chem. Chem. Phys.* **2015**, *17*, 22367-22376, DOI: 10.1039/ C5CP02453F

[23] Zhang, G.; Zhao, J.; Chow, P. C. Y.; Jiang, K.; Zhang, J.; Zhu, Z.; Zhang, J.; Huang, F.; Yan, H., Non fullerene Acceptor Molecules for Bulk Heterojunction Organic Solar Cells. *Chem. Rev.* **2018**, *118*, 3447-350,7 DOI: 10.1021/acs.chemrev.7b00535.

[24] Li, C.; Fu, H.; Xia, T.; Sun, Y., Asymmetric Non fullerene Small Molecule Acceptors for Organic Solar Cells. *Adv. Energy Mater.* **2019**, *9*, 1900999, DOI: 10.1002/aenm.201900999.

[25] Luo, Z.; Liu, T.; Yan, H.; Zou, Y.; Yang, C., Isomerization Strategy of Non fullerene Small-Molecule Acceptors for Organic Solar Cells. *Adv. Funct. Mater.* **2020**, *30*, 2004477, DOI: 10.1002/adfm.202004477.

[26] Majeed, M.; Waqas, M.; Mehmood, R. F.; Alatawi, N. S.; Essid, M.; Khera, R. A., Modified optoelectronic parameters by end-group engineering of A-D-A type non-fullerene-based small symmetric acceptors constituting IBDT core for high-performance photovoltaics. *J. Phys. Chem. Solids*, **2023**, *181*, 111495. DOI: 10.1016/ j.jpcs.2023.111495.

[27] Miao, J.; Meng, B.; Liu, J.; Wang, L., An A–D–A′–D–A type small molecule acceptor with a broad absorption spectrum for organic solar cells. *Chem. Commun.* **2018**,

*54*, 303-306. DOI: 10.1039/C7CC08497H.

[28] Yuan, J.; Zhang, Y.; Zhou, L.; Zhang, G.; Yip, H. -L.; Lau, T. -K.; Lu, X.; Zhu, C.; Peng, H.; Johnson, P. A.; Leclerc, M.; Cao, Y.; Ulanski, J.; Li, Y.; Zou, Y., Single-Junction Organic Solar Cell with over 15% Efficiency Using Fused-Ring Acceptor with Electron-Deficient Core. *Joule*, **2019**, *3*, 1140-1151, DOI: 10.1016/j.joule.2019.01.004.

[29] Zulfiqar, A., Malik, A. A.; Fan, H.; Zhu, X., Effect of terminal fluorination of indenoindene-cored non-fullerene molecular acceptors for photovoltaic application. Dyes Pigm. **2023**, *220*, 111657, DOI: 10.1016/j.dyepig.2023.111657.

[30] Agwamba, E. C.; Louis, H.; Unimuke, T. O.; Ameuru, U. S.; Mathias, G. E.; Chukwu, U. G.; Obojor-Ogar, L.; Undiandeye, U. J.; Eno, E. A., Molecular modeling of the photovoltaic properties of amino naphthalene and N-alkylated-isoquinoline dye. *J. Indian Chem. Soc.* **2022**, *99*, 100739, DOI: 10.1016/j.jics.2022.100739.

[31] Etabti, H.; Fitri, A.; Benjelloun, A. T.; Benzakour, M.; Mcharfi, M., Efficient tuning of benzocarbazole based small donor molecules with D-π-A-π-D configuration for high-efficiency solar cells via π-bridge manipulation: A DFT/TD-DFT study. *Comp. Theor. Chem.* **2021**, *1208*, 113580, DOI: 10.1016/j.comptc.2021.113580.

[32] Frisch, M. J.; Trucks, G. W.; Schlegel, H. B.; Scuseria, G. E.; Robb, M. A.; Cheeseman, J. R.; Montgomery, J. A.; Vreven, T.; Kudin, K. N.; Burant, J. C.; Millam, J. M.; Iyengar, S. S.; Omasi, J.; Barone, V.; Mennucci, B.; Cossi, M.; Scalmani, G.; Rega, N.; Petersson, G. A.; Nakatsuji, H.; Hada, M.; Ehara, M.; Toyota, K.; Fukuda, R.; Hasegawa, J.; Ishida, M.; Nakajima, T.; Honda, Y.; Kitao, O.; Nakai, H.; Klene, M.; Li, X.; Knox, J. E.; Hratchian, H. P.; Cross, J. B.; Bakken, V.; Adamo, C.; Jaramillo, J.; Gomperts, R.; Stratmann, R. E.; Yazyev, O.; Austin, A. J.; Cammi, R.; Pomelli, C.; Ochterski, J. W.; Ayala, P. Y.; Morokuma, K.; Voth, G. A.; Salvador, P.; Dannenberg, J. J.; Zakrzewski, V. G.; Dapprich, S.; Daniels, A. D.; Strain, M. C.; Farkas, O.; Malick, D. K.; Rabuck, A. D.; Raghavachari, K.; Foresman, J. B.; Ortiz, J. V.; Cui, Q.; Baboul, A. G.; Clifford, S.; Cioslowski, J.; Stefanov, B. B.; Liu, G.; Liashenko, A.; Piskorz, P.; Komaromi, I.; Martin, R. L.; Fox, D. J.; Keith, T.; Laham, A. M. A.; Peng, C. Y.; Nanayakkara, A.; Challacombe, M.; Gill, P. M. W.; Johnson, B.; Chen, W.; Wong, M. W.; Gonzalez, C.; Pople, J. A., Gaussian 09, Revision A02 (Gaussian Inc, Wallingford, **2009**).

[33] Cao, H.; Pan, X.; Li, C.; Zhou, C.; Deng, F.; Li, T., Density functional theory calculations for resveratrol. *Bioorg. Med. Chem. Lett.* **2003**, *13*, 1869-1871, DOI: 10.1016/S0960-894X(03)00283-X.

[34] Azaid, A.; Abram, T.; Kacimi, R.; Sbai, A.; Lakhlifi, T.; Bouachrine, M., Organic materials based with D–π–A structure based on thiophene and anthracene for application in dye-sensitized solar cells. *Mater. Today: Proc.* **2021**, *45*, 7363-7369, DOI: 10.1016/j.matpr.2021.01.119.

[35] Franco, F. C.; Padama, A. A. B., DFT and TD-DFT study on the structural and optoelectronic characteristics of chemically modified donor-acceptor conjugated oligomers for organic polymer solar cells. *Polymer,* **2016**, *97*, 55-62, DOI: 10.1016/j.polymer.2016.05.025.

[36] Tomasi, J.; Mennucci, B.; Cances, E., The IEF version of the PCM solvation method: : an overview of a new method addressed to study molecular solutes at the QM ab initio level, *J. Mol. Struct. THEOCHEM.* **1999**, *464*, 211, DOI: 10.1016/S0166-1280(98)00553-3.

[37] A.; Klamt, C.; Moya, J., Palomar, A Comprehensive Comparison of the IEFPCM and SS(V)PE Continuum Solvation Methods with the COSMO Approach, *J. Chem. Theor. Comput.* **2015**, *11*, 4220, DOI: 10.1021/acs.jctc.5b00601.

[38] Bagher, A. M.; Vahid, M. M. A.; Mohsen, M., Types of solar cells and application. *Am. J. Opt. Photon*. **2015**, *3*, 94-113. DOI: 10.11648/j.ajop.20150305.17.

[39] Pan, M. -A.; Lau, T. -K.; Tang, Y.; Wu, Y. -C.; Liu, T.; Li, K.; Chen, M. -C.; Lu, X.; Ma, W.; Zhan, C., 16.7%-efficiency ternary blended organic photovoltaic cells with PCBM as the acceptor additive to increase the open-circuit voltage and phase purity. *J. Mater. Chem. A.* **2019**, *7*, 20713-20722, DOI: 10.1039/C9TA06929A.

[40] Hussain, R.; Khan, M. U.; Mehboob, M. Y.; Khalid, M.; Iqbal, J.; Ayub, K.; Adnan, M.; Ahmed, M.; Atiq, K.; Mahmood, K., Enhancement in Photovoltaic Properties of *N*,*N*-diethylaniline based Donor Materials by Bridging Core Modifications for Efficient Solar Cells. *Chem. Select.* **2020**, *5*, 5022, DOI: 10.1002/slct.202000096.

[41]Nebbach, D.; Agda, F.; Kaya, S.; Siddique, F.; Lakhlifi, T.; Ajana, M. A.; Bouachrine, M., Non-fullerene acceptor IDIC based on indacinodithiophene used as an electron donor for organic solar cells: A computational study, *J. Mol. Liq.* **2022**, *348*, 118289, DOI: 10.1016/j.molliq.2021.118289.

[42] Kacimi, R.; Tanıs, E.; Azaid, A.; Khaddam, Y.; Raftani, M.; Sarfaraz, S.; Bejjit, L.; Bouachrine, M., Benzodithiophene-based Acceptor-Donor-Acceptor-type compounds for highly efficient organic photovoltaic cells. *Chem. Phys. Lett.* **2023**, *830*, 140774, DOI: 10.1016/j.cplett.2023.140774 .

[43] Britel, O.; Etabti, H.; Fitri, A; Benjelloun, A. T.; Benzakour, M.; Mcharfi, M., Computational studies of the influence of auxiliary acceptors in the D-A'-π-A structure of organic dyes on the photovoltaic performance of dye solar cells, *J. Mol. Model.* **2024**, *30*, 70, DOI: 10.1007/s00894-024-05871-x.

[44] Ninis, O.; Kacimi, R.; Bouaamlat, H.; Abarkan, M.; Bouachrine, M., Theoretical studies of photovoltaic properties for design of new Azo-Pyrrole photo-sensitizer materials as dyes in solar cells, *J. Mater. Environ. Sci.* **2017**, *8*, 2572-2578.

[45] Prakasam, M.; Baskar, R.; Gnanamoorthi, K.; Annapoorani, K., Triphenylamine Based Organic Dyes with Different Spacers for Dye-Sensitized Solar Cells: A First Principal Study. *Int. J. Adv. Sci. Eng.* **2019**, *5*, 1118, DOI: 10.29294/IJASE.5.4.2019.1118-1124.

[46] Khan, M. U.; Khalid, M.; Khera, R. A.; Akhtar, M. N.; Abbas, A.; Rehman, M. F.; Braga, A. A. C.; Alam, M. M.; Imran, M.; Wang, Y.; Lu, C., Influence of acceptor tethering on the performance of nonlinear optical properties for pyrene-based materials with A-π-D-π-D architecture. *Arabian J. Chem.* **2022**, *15*, 103673, DOI: 10.1016/j.arabjc.2021.103673.

[47] Etabti, H.; Fitri, A; Benjelloun, A. T.; Benzakour, M.; Mcharfi, M., Advancing optoelectronic performance of organic and perovskite photovoltaics: computational modeling of hole transport material based on end-capped dibenzocarbazole molecules, *Res. Chem. Intermed.* **2024**, *50*, 1895-1927, DOI: 10.1007/s11164-024-05244-2.

[48] Khan, M. U.; Mehboob, M. Y.; Hussain, R.; Fatima, R.; Tahir, M. S.; Khalid, M.; Braga, A. A. C., Molecular designing of high-performance 3D star-shaped electron acceptors containing a truxene core for non-fullerene organic solar cells. *J. Phys. Org. Chem.* **2021**, *34*, e4119, DOI: 10.1002/poc.4119.

[49] Etabti, H.; Fitri, A.; Benjelloun, A. T.; Hachi, M.; Benzakour, M.; Mcharfi, M., Benzocarbazole–based D-Di–π–A dyes for DSSCs: DFT/TD–DFT study of influence of auxiliary donors on the performance of free dye and dye–$TiO_2$ interface. *Res. Chem. Intermed.* **2021**, *47*, 4257-4280, DOI: 10.1007/s11164-021-04531-6.

[50] Ali, U.; Etabti, H.; Muhammad Rizwan Ahmad, H.; Uz Zafar, S., The conformational control of small D-A-D organic solar cells for large power conversion efficiency: A deep quantum chemistry analysis. *Comp. Theor. Chem.* **2022**, *1215*, 113831, DOI: 10.1016/j.comptc.2022.113831.

[51] Etabti, H.; Fitri, A.; Benjelloun, A. T.; Benzakour, M.; Mcharfi, M., Effects of the terminal donor unit on the photovoltaic parameters of benzocarbazole-based dyes for DSSCs: DFT/TD-DFT investigations. *E3S Web Conf.* **2022**, *336*, 00031, DOI: 10.1051/e3sconf/202233600031.

[52] Etabti, H.; Fitri, A.; Benjelloun, A. T.; Benzakour, M.; Mcharfi, M., Designing and Theoretical Study of Dibenzocarbazole Derivatives Based Hole Transport Materials: Application for Perovskite Solar Cells. *J. Fluoresc.* **2023**, *33* (3), 3. DOI: 10.1007/s10895-023-03144-z.

[53] Etabti, H.; Fitri, A.; Benjelloun, A. T.; Benzakour, M.; Mcharfi, M., A DFT/TD-DFT Study of the Influence of Anchoring Group and Internal Acceptor of Benzocarbazole-based D-A´-π-A Dyes for DSSCs. *Int. J. Comput. Theor. Chem.* **2024**, *12*, 1-9, DOI: 10.11648/j.ijctc.20241201.11.

[54] Rashid, E. U.; Iqbal, J.; Mehmood, R. F.; El-bardy, Y. A.; Akram, S. J.; Khera, R. A., Depicting the role of end-capped acceptors to amplify the photovoltaic properties of benzothiadiazole core-based molecules for high-performance organic solar cell applications. *Comp. Theor. Chem.* **2022**, *1211*, 113669, DOI: 10.1016/j.comptc.2022.113669.

[55] Kayani, K. Q.; Yaqoob, U.; Jabeen, S.; Iqbal, S.; Yaseen, M.; Khalid, M.; Akhter, M. S.; Iqbal, J., Tris-isopropyl-sily-ethynyl anthracene based small molecules for organic solar cells with efficient photovoltaic parameters. *Comp. Theor. Chem.* **2021**, *1202*, 113305, DOI:

10.1016/j.comptc.2021.113305.

[56] Shehzad, R. A.; Iqbal, J.; Khan, M. U.; Hussain, R.; Javed, H. M. A.; Ur Rehman, A.; Alvi, M. U.; Khalid, M., Designing of benzothiazole based non-fullerene acceptor (NFA) molecules for highly efficient organic solar cells. *Comp. Theor. Chem.* **2020**, *1181*, 112833, DOI: 10.1016/j.comptc.2020.112833.

[57] Kim, B.; Yeom, H. R.; Yun, M. H.; Kim, J. Y.; Yang, C., A selenophene analogue of PCDTBT: Selective fine-tuning of lumo to lower of the bandgap for efficient polymer solar cells. *Macromolecules*, **2012**, *45*, 8658-8664, DOI: 10.1021/ma302133h.

[58] An, Q.; Zhang, F.; Zhang, J.; Tang, W.; Deng, Z.; Hu, B., Versatile ternary organic solar cells: a critical review. *Energy Environ. Sci.* **2016**, *9*, 281-322, DOI: 10.1039/C5EE02641E.

[59] Yousaf, I.; Khera, R. A.; Iqbal, J.; Gul, S.; Jabeen, S.; Ihsan, A.; Ayub, K., Isatin-derived non-fullerene acceptors for efficient organic solar cells. *Mat. Sci. Semicond. Process.* **2021**, *121*, 105345, DOI: 10.1016/j.mssp.2020.105345.

[60] Zubair, I.; Kher, R. A.; Akram, S. J.; El-badry, Y. A.; Saeed, M. U.; Iqbal, J., Tuning the optoelectronic properties of indacenodithiophene based derivatives for efficient photovoltaic applications: a DFT approach. *Chem. Phys. Lett.* **2022**, *793*, 139459, DOI: 10.1016/j.cplett.2022.139459.

[61] Duan, Y. A.; Geng, Y.; Li, H. B.; Jin, J. L.; Wu, Y.; Su, Z. M., Theoretical characterization and design of small molecule donor material containing naphthodithiophene central unit for efficient organic solar cells. *J. Comput. Chem.* **2013**, *34*, 1611-1619, DOI: 10.1002/jcc.23298.

[62] Etabti, H.; Fitri, A.; Benjelloun, A. T.; Benzakour, M.; Mcharfi, M., Designing and theoretical study of benzocarbazole-based D-π-D type small molecules donor for organic solar cells. *J. Mol. Graph. Model.* **2023**, *121*, 108455. DOI: 10.1016/j.jmgm.2023.108455.

[63] Gadisa, A.; Svensson, M.; Andersson, M. R.; Inganas, O., Correlation between oxidation potential and open-circuit voltage of composite solar cells based on blends of polythiophenes/fullerene derivative. *Appl. Phys. Lett.* **2004**, *84*, 1609-1611. DOI: 10.1063/1.1650878.

[64] Dou, L.; Liu, Y.; Hong, Z.; Li, G.; Yang, Y., Low-bandgap near-IR conjugated polymers/molecules for organic electronics. *Chem. Rev.* **2015**, *115*, 12633- 12665. DOI: 10.1021/acs.chemrev.5b00165.

[65] Agda, F.; Taleb, M.; Abram, T.; Bejjit, L.; Bouachrine, M., Materials Based on Carbazole for Organic Solar Cells Applications. Theoretical Investigations. *Phys. Chem. Res.* **2014**, *2* (2), 244-251. DOI: 10.22036/pcr.2014.6071.

[66] McGehee, M. D.; Cates, N. C.; Gysel, R.; Dahl, J. E. P.; Sellinger, A., Effects of intercalation on the hole mobility of amorphous semiconducting polymer blends. *Chem. Mater.* **2010**, *22*, 3543-3548. DOI: 10.1021/ cm1008619.

[67] Koster, L. J. A.; Mihailetchi, V. D.; Blom, P. W. M., Ultimate efficiency of polymer/fullerene bulk heterojunction solar cells. *Appl. Phys. Lett.* **2006**, *88*, 1-4. DOI: 10.1063/1.2181635.